Cyclic Voltammetry of Semiconductor Photoelectrodes III: A Comparison of Experiment and Theory for *n*-Si and *p*-Si Electrodes

Patrick G. Santangelo, Marya Lieberman, and Nathan S. Lewis*

Division of Chemistry and Chemical Engineering, California Institute of Technology, Pasadena, California 91125

Received: November 4, 1997; In Final Form: February 18, 1998

Cyclic voltammograms have been obtained under a variety of conditions using a semiconducting photoelectrode or a circuit containing a diode in series with a metallic electrode. Simulations of the voltammetry of both types of systems were performed using a model circuit in which electrode nonideality, double-layer capacitance, and parallel resistance effects were accounted for quantitatively. The simulated voltammograms were in excellent agreement with the experimental data for a diode/electrode circuit, yielding a reliable description of the shapes of the voltammograms as well as of the voltage dropped across the diode element as a function of the total potential dropped across the circuit. The digital simulations were in good agreement with the voltammetry of *p*-Si/$CH_3OH-CoCp_2^{+/0}$ contacts at high light intensities, but could not quantitatively describe the shapes of the voltammograms at low light intensities.

I. Introduction

We have previously presented working curves for the voltammetry of semiconductors in both rotating disk and planar electrode geometries.[1,2] These working curves established that a dimensionless parameter, θ, was sufficient to characterize the steady-state voltammetry of rotating disk electrodes and the cyclic voltammetry of electrodes with surface-attached electroactive species or freely diffusing redox reagents. The parameter θ has been shown analytically to reflect the ratio of the dynamic impedance of a semiconductor diode element to the faradaic impedance of the interfacial charge-transfer process.

To develop this analytical model, the semiconductor electrode was modeled using an equivalent circuit formalism. In this formalism, the system was broken down into an ideal diode connected electrically in series with a metal electrode/electrolyte contact.[1−6] This treatment facilitated separation of the theoretical problem into two components, one of which described the interfacial component of the current and the other of which accounted for the nonlinear impedance characteristics of the diode. This prior work demonstrated that a variety of unconventional shapes for cyclic voltammograms at semiconductor electrodes could be interpreted and analyzed quantitatively as a function of the dimensionless parameter θ.

To date it appears, however, that no experimental voltammetry of a freely diffusing electroactive species at a semiconductor electrode has been described with sufficient precision to test rigorously the predictions of this model. In this manuscript we present the results of such voltammetric experiments. In addition, we report the experimental behavior of a diode in series with a metal electrode/electrolyte redox couple, and compare both sets of experimental data with the predictions of the analytical model.

II. Modifications of Previous Theory

Several modifications of the published theory[1,2] were required to simulate adequately the behavior of experimental voltammograms. For conceptual simplicity, the prior theory ignored the presence of any double-layer capacitance, solution resistance, parallel leakage currents, or contacts having nonideal diode quality factors. The inclusion of these factors was critical for satisfactorily modeling experimental data. A new set of simulations was therefore generated to model these additional experimental features.

A. Semiconducting Electrode Simulations. *1. Equivalent Circuit Modifications.* The equivalent circuit used in this work is shown schematically in Figure 1. Relative to prior models, additional circuit elements account for the effects of capacitance at the metal electrode/solution interface (C_d), background currents (Z), and any series resistance losses in the electrolyte (R_s).

The externally applied voltage (V_s) produced voltage drops across both the photoactive element (V_d) and the electrochemical cell (V_e). It also produced a series resistance loss in the electrolyte, I_sR_s, with I_s representing the current flowing in the solution. The voltages in the circuit were all explicit functions of time, and had the relationship:

$$V_s = V_d + V_e + I_sR_s \tag{1}$$

Including capacitive currents as well as parallel resistance (leakage currents) and faradaic currents in the system produced an additional constraint on the circuit model:

$$I_s = I_d = (I_e + I_c + I_z) \tag{2}$$

where I_s, I_d, and I_e refer to the current flowing through the system, diode, and metal electrode, respectively.

Within the circuit model, I_c and I_z represent two components of the background current of an actual experimental system. I_c is proportional to the scan rate and is independent of the applied potential. Previously, eq 3 allowed determination of I_c from experimental voltammograms:

$$I_c = A_sC_dv_e \tag{3}$$

In this equation, A_s is the electrode area, C_d is the differential capacitance, and v_e is the scan rate of the potential applied to

S1089-5647(98)00073-X CCC: $15.00
Published on Web 05/22/1998

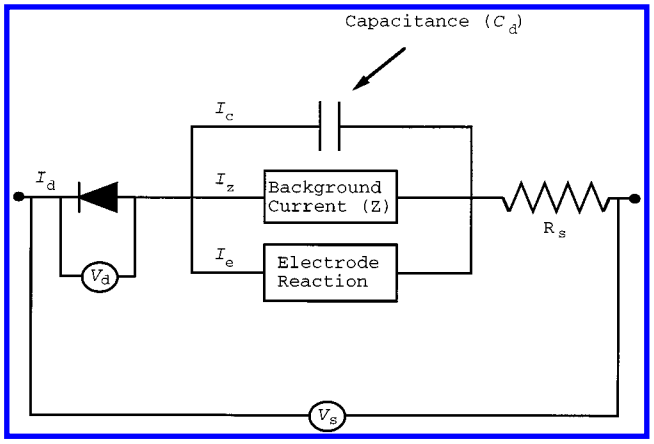

Figure 1. The equivalent circuit used as a model for the ideal semiconductor/liquid interface, including the effects of capacitance at the metal electrode/solution interface (C_d), background current (Z), and series resistance losses in the electrolyte (R_s).

the metal electrode. I_z was taken as the residual component of the background current that depended on both potential and scan rate, and was satisfactorily described by:

$$I_z = \frac{\sqrt{|v_e|}}{R'}(V_e - V_{z,\text{initial}}) + I_{z,\text{initial}} \tag{4}$$

where for the forward scan direction of V_e

$$V_{z,\text{initial}} = V_{e,\text{initial}} \quad \text{and} \quad I_{z,\text{initial}} = 0 \tag{5a}$$

and where for the reverse scan direction of V_e

$$V_{z,\text{initial}} = V_{e,\,\max} \quad \text{and} \quad I_{z,\text{initial}} = I(V_{e,\max}) \tag{5b}$$

In eqs 5a and 5b, $V_{e,\text{initial}}$ is the potential across the metal electrode at $t = 0$, $V_{e,\max}$ is the potential at the metal electrode when the scan direction is reversed, and $I(V_{e,\max})$ is the value of the current at $V_e = V_{e,\max}$. The parallel reaction coefficient, R', is an empirically determined constant that reflects the scan rate dependence of the background current. The value of R' was approximated as:

$$R' = \frac{dV_e}{dI_e}\sqrt{v_e} \tag{6}$$

with R' expressed in units of $\Omega(s/V)^{1/2}$.

2. Simulation Equations and Methodology. Analysis of this circuit model consisted of solving for I_e as a function of V_s. This problem is very similar to that described in the previous ideal circuit description.[1,2] Because this new model circuit had nonlinear responses to voltage, the current−voltage behavior of the system was solved numerically rather than analytically.

A digital simulation technique was used to obtain the desired numerical solution.[8] The boundary conditions at a metal electrode interface for a reversible redox reaction $R \leftrightarrow O + ne^-$, where $O(x, t) = 0$ for $x \geq 0$ and $t = 0$, are given by eqs 7−10:[7]

$$\phi_e \equiv e^{[nF(V_e - E^{\circ\prime})/RT]} = \frac{O(0,t)}{R(0,t)} \tag{7}$$

$$f_R = D_R(R_1 - R_0)/\Delta x_1 \tag{8}$$

$$f_O = D_O(O_1 - O_0)/\Delta x_1 \tag{9}$$

$$f_R = -f_O \tag{10}$$

where $E^{\circ\prime}$ is the formal redox potential of the system, D_R and D_O are the diffusion coefficients of the reduced and oxidized forms of the redox species, respectively, R_1 and O_1 are the concentrations of O and R in the first volume element, respectively, R_0 and O_0 are the concentrations of O and R at the electrode surface, respectively, f_R and f_O are the respective fluxes of reduced and oxidized material, and Δx_1 is the distance between the position of the average concentration in the first volume element and the position of the plane of the electrode.

When the diode equation

$$I(V_d) = I_L - I_0[e^{-qV_d/AkT} - 1] \tag{11}$$

with I_L the limiting photocurrent and I_0 the exchange current of the diode, and eqs 2 and 7−10 are substituted into the voltage constraint of eq 1, the following expression is obtained for the flux, $f_R(t)$, through the metal electrode at time t:

$$\left[\frac{R_1 - \frac{\overline{\Delta x_1}\, f_R}{D_R}}{O_1 - \frac{\overline{\Delta x_1}\, f_R}{D_O}}\right]\phi_s = \left[\frac{I_0}{I_L + I_0 - (nFA_s f_R + I_c + I_z)}\right]e^{((nFR_s/RT)(nFA_s f_R + I_c + I_z))} \tag{12}$$

As in a previous treatment, ϕ_s is expressed as:

$$\phi_s = e^{[nF(V_s - E^{\circ\prime})/RT]} \tag{13}$$

For eqs 3 and 4, the finite-difference approximation to the scan rate of the applied potential across the metal electrode, v_e, was given by

$$v_e = (V_e(t) - V_e(t - \Delta t))/\Delta t \tag{14}$$

The parameter $V_e(t)$ may be derived from eq 14 and from the flux of the reduced species, f_R, whose value is calculated as shown in eq 15:

$$f_R = \frac{\phi_e(R_1 - O_1)}{\frac{\Delta x_1}{D_O} + \frac{\phi_e \Delta x_1}{D_R}} \tag{15}$$

Once the flux at the electrode surface, $f_R(t)$, was numerically determined for a given time t, the current flowing through the metal electrode element was readily calculated from the relation $I_e(t) = nFA_s f_R(t)$. Equations 3 and 4 were then used to calculate the remaining components of the current, $I_c(t)$ and $I_z(t)$. The total current $I_s(t)$ was obtained by substituting the values of $I_e(t)$, $I_c(t)$, and $I_z(t)$ into eq 2, followed by the calculation of the value of V_d from the direct substitution of I_s (= I_d) into eq 11. Using this procedure, the entire cyclic voltammetric response was generated as a function of V_s for specific values of R', C_d, R_s, A, I_o, I_L, v, D_O, D_R, and A_s.

B. Metal Electrode Simulations. Simulations were also developed for a simple system consisting of a single metal electrode with no diode in the circuit. These simulations included the effects of background current, capacitance at the electrode/solution interface, and series resistance losses in the electrolyte. To treat this case, a finite-difference equation describing the flux at a given electrode voltage ($V_e(t)$) was derived using an equivalent circuit formalism for the reversible redox reaction $R \leftrightarrow O + ne^-$.

The derivation followed the general approach already described, with the exception that the system constraints were

given by

$$V_s = V_e + I_s R_s \tag{16}$$

and

$$I_s = (I_e + I_c + I_z) \tag{17}$$

Substituting eqs 7−10 and 17 into eq 16 yielded the following general finite-difference expression for the flux, $f_R(t)$, through the metal electrode at time t:

$$\begin{bmatrix} R_1 - \dfrac{\overline{\Delta x_1} f_R}{D_R} \\ O_1 - \dfrac{\overline{\Delta x_1} f_R}{D_O} \end{bmatrix} \phi_s = e^{((nFR_s/RT)(nFA_s f_R + I_c + I_z))} \tag{18}$$

In this equation, ϕ_s, I_c, and I_z are given by eqs 13, 3, and 4, respectively.

The current I_e was readily obtained through use of the relation $I_e(t) = nFA_s f_R(t)$. The remaining components of the current, $I_c(t)$ and $I_z(t)$, were determined from eqs 3 and 4, and the total current $I_s(t)$ was determined by substituting the values of $I_e(t)$, $I_c(t)$, and $I_z(t)$ into eq 2. Using this procedure, the entire cyclic voltammetric response was generated as a function of V_s for specific values of R', C_d, R_s, υ, D_O, D_R, and A_s.

III. Experimental Section

The voltammograms in this study were recorded using a conventional anaerobic, three-electrode configuration.[9−11] The reference electrode was a methanolic saturated calomel electrode (MSCE), against which the formal potential, $E^{\circ\prime}$, of 1,1′-dimethylcobaltocenium (Me_2CoCp_2)PF_6 was measured as −1.00 V. The counter electrode was a Pt flag electrode. Voltammetric scans were initiated at the positive voltage limit.

Voltammetry was performed using a Princeton Applied Research Model 173/175 Potentiostat/Programmer combination equipped with a PAR Model 179 Digital Coulometer. The 1,1′-$Me_2CoCp_2PF_6$ was synthesized and purified as described in the literature. $CoCp_2PF_6$ was prepared as described previously[9] and was purified by recrystallization. Me_2Fc was prepared and purified as described previously.[12]

Semiconductor electrodes were prepared from 1.5 ohm-cm resistivity, (100)-oriented, *n*-type Si or from 1.5 ohm-cm resistivity, (100)-oriented, *p*-type Si wafers. The wafers were sliced into 4 × 4 mm squares, and each square was fabricated into an ohmically contacted electrode as described previously.[12] Each electrode was etched in 48% HF(aq), rinsed with H_2O, then rinsed with solvent, and dried under N_2(g) immediately before use.

A Luggin capillary was fabricated from a commercial disposable Pasteur pipet that had been modified to have a tip diameter of ≈0.1 mm. A MSCE was placed into the top of the Luggin capillary, and the entire electrode asssembly was immersed into the electrochemical cell through a ground glass fitting in the top of the cell. Illumination for all experiments was obtained from an ELH bulb, with the light intensity varied by inserting Hoya neutral density filters between the lamp and the electrode.

Fits were extracted from experimental voltammogram curves with the Levenberg−Marquardt nonlinear least-squares algorithm.[13−15] Because the model depended nonlinearly on the set of unknown parameters, a figure of merit was defined, and its minimization determined the best-fit parameters. The adjustable parameters were changed by a fixed amount for each iteration until the figure of merit was constant for a specific number of iterations; this distiguished global from local minima. The exact procedure used in the minimization process is beyond the scope of this work, and the interested reader is referred to the literature already noted for a complete description of the Levenberg−Marquardt nonlinear least-squares algorithm. All calculations were performed on an Apple Macintosh SE equipped with an Irwin Magnetic 68020/68881/68851 accelerator board using Absoft Corp. MacFortran/020.

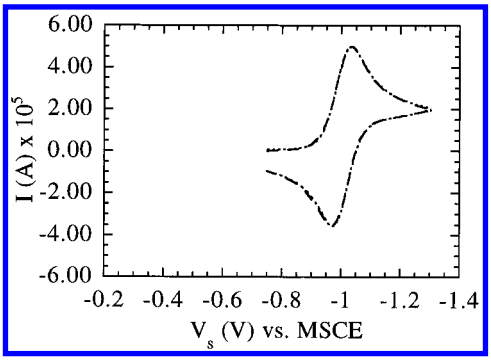

Figure 2. Cyclic voltammogram of the Pt/CH_3CN−1.0 M $TEABF_4$−1.2 mM $Me_2CoCp_2PF_6$ interface at a potential scan rate of 100 mV s^{-1}. The applied potential, V_e, was referenced to a methanolic SCE, and $E^{\circ\prime}$ was measured as −1.00 V versus MSCE. Cathodic currents are positive. The values for all simulation parameters are given in Table 1. Key: (dashed curve) experimental; (dotted curve) simulation.

The model circuit can be used to simulate either *n*-type or *p*-type semiconductors. Thus, when the diode is oriented in the circuit so that photocurrent is cathodic, the series diode/electrode combination models a *p*-type semiconductor photocathode. In all figures, cathodic current lies above zero on the I axis and reverse bias, meaning more negative values of V_s, lies toward the right on the V_s axis. This reversal of the IUPAC convention was made to facilitate comparison of the curve shapes with the previous simulations, which were performed for an *n*-type semiconductor and for which reverse bias corresponded to more positive potentials.

IV. Results

A. Simulation of Cyclic Voltammetry for the Metal/Solution Circuit. Figure 2 displays the experimental cyclic voltammetric response (dashed curve) of the Pt/CH_3CN−1.0 M $TEABF_4$−1.2 mM $Me_2CoCp_2PF_6$ interface at a potential scan rate of 100 mV s^{-1}. The cyclic voltammogram was characterized by a difference between anodic and cathodic peak potentials, $\Delta E_{p,m}$, of 62 mV, and a cathodic peak width, $\Delta E_{p/2,m}$, of 60 mV (as determined by the points where $I = I_{pc,m}$ and $I = I_{pc,m}/2$). A small uncompensated resistance would account for the small deviations observed in $\Delta E_{p,m}$ and $\Delta E_{p/2,m}$ from the Nernstian, one-electron values of 57 and 58 mV, respectively. The cathodic peak current, $I_{pc,m}$, deviated slightly from the expected linear dependence on the square root of the scan rate for rates between 2 and 200 mV s^{-1}.

The simulated voltammogram is shown as the dotted curve in Figure 2. Values for the redox couple concentration, the metal electrode area,[9,10] and the diffusion constants[7,16] used in the digital simulation were independently determined; the values used are listed in Table 1. Values of the capacitance (C_d), the uncompensated resistance (R_s), and the parallel reaction coefficient (R') were adjusted until the best fit to this set of experimental data was obtained (Table 1).

Although these values were obtained from the cyclic voltammogram at 100 mV s^{-1}, they also provided excellent fits to

TABLE 1: Values Used in Simulations for Cyclic Voltammetric Behavior at Pt Electrode in 1.0 M $TEABF_4$−1.2 mM $Me_2CoCp_2PF_6$−CH_3CN

parameter	value
bulk conc of reductant	1.2×10^{-6} mol/cm^3
no. of electrons in reaction	1.00
formal potential of electroactive material	−1.00 V versus MSCE
diffusion coeff of reduced and oxidized species	1.74×10^{-5} cm^2/s
sweep rate	0.10 V/s
area of electrode	0.107 cm^2
temperature	25.00 °C
differential capacitance	54.2 μF/cm^2
series resistance	29.1 Ω
parallel reaction coeff	8.7×10^4 Ω(s/V)$^{1/2}$

TABLE 2: Values Used in Simulations for Cyclic Voltammetric Behavior at Pt Electrode in 1.0 M $TEABF_4$−4.5 mM $CoCp_2PF_6$−CH_3CN

parameter	value
bulk conc of reductant	4.5×10^{-6} mol/cm^3
no. of electrons in reaction	1.00
formal potential of electroactive material	−0.89 V versus MSCE
diffusion coeff of reduced and oxidized species	1.8×10^{-5} cm^2/s
sweep rate	0.10 V/s
area of electrode	0.0633 cm^2
temperature	25.00 °C
differential capacitance	2.54×10^2 μF/cm^2
series resistance	30.8 Ω
parallel reaction coeff	2.5×10^4 Ω(s/V)$^{1/2}$

the data obtained at scan rates between 2 and 200 mV s^{-1}, indicating that the simulation methodology was valid over our range of experimental parameters. In addition, the values of C_d and R_s were typical for the type of electrochemical system under investigation,[7] and the best-fit value of $R' = 8.7 \times 10^4$ Ω(s/V)$^{1/2}$ obtained from the simulation was close to the value of $R' = 1.1 \times 10^5$ Ω(s/V)$^{1/2}$ obtained experimentally from the background current−voltage data in this electrolyte. Because of the satisfactory agreement between simulations and experimental data, further simulations of this system, including simulations of the metal electrode component of the *p*−*n* photodiode/Pt metal electrode/$Me_2CoCp_2PF_6$ redox system, used the quantities given in Table 1 as standard, unadjustable parameters.

The simulation was also used to generate theoretical cyclic voltammograms for a different redox couple, the Pt/CH_3CN−1.0 M $TEABF_4$−4.5 mM $CoCp_2PF_6$ interface. This redox couple will be further discussed in *Section IV. D.* Values of the redox couple concentration, the metal electrode area, and the diffusion constants (shown in Table 2), were used in the Levenberg−Marquardt algorithm as fixed parameters. Values of the capacitance (C_d), the uncompensated resistance (R_s), and the parallel reaction coefficient (R') were then adjusted until the best fit to the experimental data was obtained, with the resulting quantities listed in Table 2. The values obtained were quite reasonable for a electrode/electrochemical system of this type.[7] The fit to the experimental data for the Pt/CH_3CN−4.5 mM $CoCp_2PF_6$−1.0 M $TEABF_4$ system was comparable in quality to the fit obtained for the Pt/CH_3CN−1.2 mM $Me_2CoCp_2PF_6$−1.0 M $TEABF_4$ system already described.

B. Cyclic Voltammetry for the Diode/Metal Electrode/Electrolyte System. Figure 3 depicts the experimental cyclic voltammetric response of a diode/electrode circuit combination. To obtain these data, the Pt/CH_3CN−1.0 M $TEABF_4$−1.2 mM $Me_2CoCp_2PF_6$ interface was placed in series electrically with an EG&G UV100−BQ *p*−*n* Si photodiode before connection to the potentiostat. The diode had been independently characterized with respect to its *I*−*V* behavior, and displayed $A = 1.34 \pm 0.04$ and $I_o = (2.90 \pm 1.64) \times 10^{-10}$ A. Cyclic voltammetric measurements of this diode/metal electrode/electrolyte system were then performed under potentiostatic control using the same Pt metal electrode and solution of Figure 2. The $I_s - V_d$ data were also collected by monitoring the current through the potentiostat while determining the voltage drop across the diode.

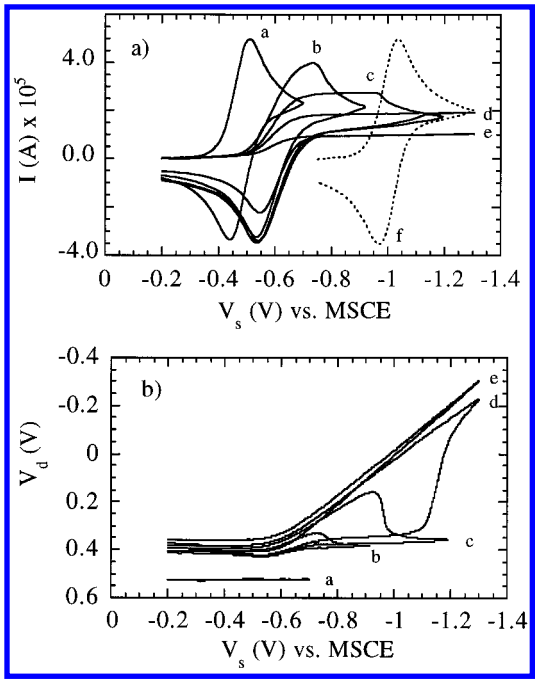

Figure 3. (a) Cyclic voltammograms of a *p*-*n*-Si photodiode in series with the Pt/CH_3CN−1.0 M $TEABF_4$−1.2 mM $Me_2CoCp_2PF_6$ electrochemical cell for various values of the light-induced current I_L. The scan rate of the applied potential was 100 mV s^{-1}, and $E^{\circ\prime}$ was measured as −1.00 V versus MSCE. Cathodic currents are positive. The values for all other parameters are given in Table 1. Curve a: $I_L = 1.17 \times 10^{-3}$ A. Curve b: $I_L = 4.40 \times 10^{-5}$ A. Curve c: $I_L = 2.82 \times 10^{-5}$ A. Curve d: $I_L = 1.88 \times 10^{-5}$ A. Curve e: $I_L = 1.00 \times 10^{-5}$ A. Curve f: The cyclic voltammogram of the Pt electrode without the *p*-*n*-Si photodiode in the circuit. (b) Plot of the voltage drop across the photodiode, V_d, as a function of the applied voltage, V_s, for voltammograms a−e already shown. All parameters are identical with those given for (a).

As the light intensity increased, the cyclic voltammetric wave shifted to more positive potentials relative to the cyclic voltammetric response of the Pt metal electrode (Figure 3). Furthermore, the wave shape of the diode/electrode hybrid approached that of a conventional Pt metal electrode, with a difference between anodic and cathodic peak potentials, ΔE_p, of 62 mV, and a cathodic peak width, $\Delta E_{p/2}$, of 60 mV. At sufficiently high illumination levels ($I_L > 1.0 \times 10^{-3}$ A), the *I*−*V* behavior of the electrochemical system was qualitatively in accord with the ideal semiconductor electrode properties predicted in prior work.[7,17]

At a high light intensity ($I_L > 1.0 \times 10^{-3}$ A), the voltage drop across the diode was essentially constant at all values of V_s, as shown by curve a in Figure 3b. The equivalent series circuit was thus dominated by faradaic processes at the metal/solution interface and not by the transport impedance of the photodiode. Under these conditions, the open-circuit voltage can be directly extracted from the shifts in E_{pa}, E_{pc}, or $E_{1/2}$

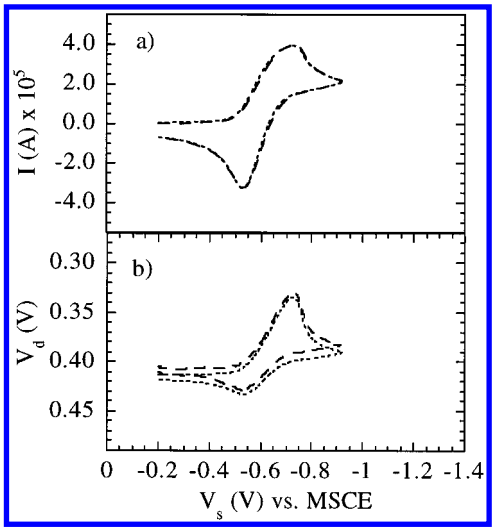

Figure 4. (a) Experimental and simulated cyclic voltammogram of a *p*−*n*-Si photodiode in series with the Pt/CH_3CN−1.0 M $TEABF_4$−1.2 mM $Me_2CoCp_2PF_6$ electrochemical cell for $I_L = 4.40 \times 10^{-5}$ A (curve b in Figure 3). Cathodic currents are positive. The values for all other parameters are given in Table 1. Key: dashed curves) experimental; (dotted curves) simulation. (b) Plot of the experimental and simulated voltage drop across the photodiode, V_d, as a function of the applied voltage, V_s, for the voltammograms shown in (a). All parameters are identical with those given for (a). Key: (dashed curves) experimental; (dotted curves) simulation.

between the illuminated photodiode/metal electrode/redox system and the Pt electrode/redox system.

For moderate light intensities ($I_L < 1.0 \times 10^{-3}$ A), the cyclic voltammetric wave shapes deviated from the response of the Pt metal electrode (Figure 3a). The value of ΔE_p increased from the Pt metal electrode value of 62 mV, and the cathodic wave broadened, shifting $\Delta E_{p/2}$ from the value of 60 mV observed at the Pt metal electrode. Furthermore, the values of $\Delta E_{1/2}$ and ΔE_{pc} became extremely large and did not provide accurate estimates of V_{oc}. In fact, ΔE_{pa} provided a better measure of V_{oc} than either $\Delta E_{1/2}$ or ΔE_{pc} under these particular conditions. This result is in accord with expectations that, at low illumination levels, the transport impedance of the photodiode should dominate the current−voltage characteristics of the diode/electrode system. At sufficiently low light intensities ($I_L < 2.0 \times 10^{-5}$ A), where a significant fraction of the applied system voltage V_s is expected to partition across the photodiode, a cathodic current plateau was observed in the current−voltage response of the series photodiode/Pt electrode/redox system (Figure 3a, curve d). The unusual curve shapes observed at low light intensities presented a challenge for the simulation that might reveal flaws in the equivalent circuit model.

C. Simulation of Cyclic Voltammetry for the Diode/Metal Electrode/Electrolyte System. The simulated current−voltage responses for the diode/electrode/liquid contact were generated by the same digital simulation technique described in *Section IV.A*, except that the flux at the electrode/solution interface was given by eq 12. The unadjustable parameters that were used for the metal electrode are listed in Table 1. The only adjustable parameters were the diode quality factor (A) and the reverse saturation current (I_o). Values for these parameters were determined by applying the Levenberg−Marquardt nonlinear least-squares algorithm to the experimental data.

At low light intensities (e.g., curve e in Figure 3), application of this fitting procedure yielded $A = 1.36$ and $I_o = 3.30 \times 10^{-10}$ A (Figure 4a, dotted curve). These values were in accord with experimental determinations of A and I_o (vide supra) and also

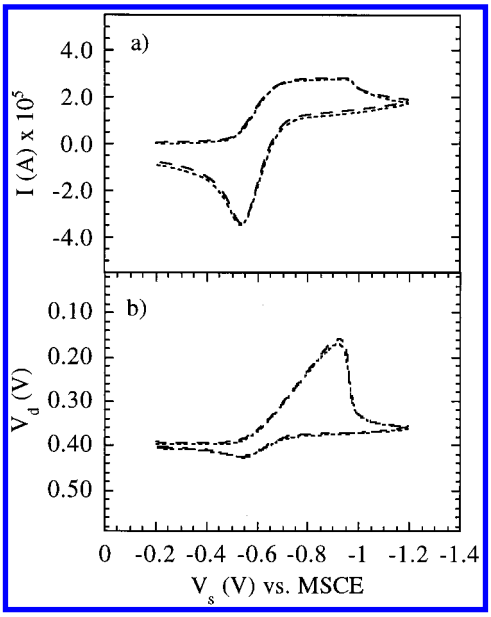

Figure 5. Experimental and simulated cyclic voltammogram for curve c in Figure 3, $I_L = 2.82 \times 10^{-5}$ A. (a) Cyclic voltammetry data. (b) Plot of the voltage drop across the photodiode, V_d, as a function of the applied voltage, V_s, for the voltammograms shown in (a).

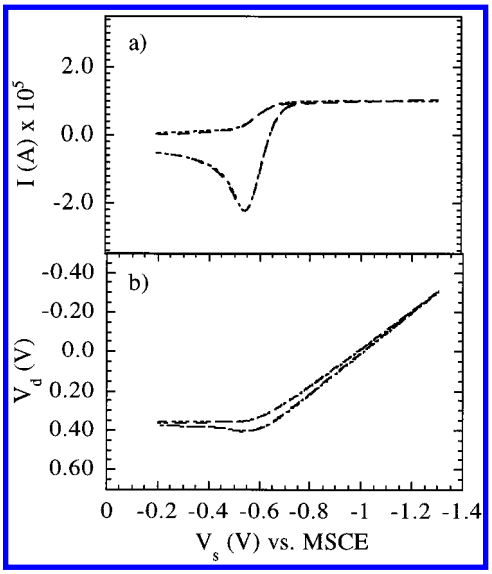

Figure 6. (a) Experimental and simulated cyclic voltammogram for curve e of Figure 3 ($I_L = 1.00 \times 10^{-5}$ A). (b) Plot of the V_d versus V_s for the voltammograms shown in (a). Key: (dashed curves) experimental; (dotted curves) simulation.

produced excellent agreement between simulated and experimental voltammograms over the entire potential scan range (Figures 4a, 5a, and 6a).

Figure 4b (dashed curve) depicts the experimentally determined voltage drop across the photodiode, V_d, as a function of the applied system voltage, V_s . By substituting the values of I_s, A, and I_o into eq 11, V_d versus V_s could also be calculated from the voltammetric data. The calculated value of V_d, shown in Figure 4b, and was in outstanding agreement with the direct experimental measurements.

To provide further evidence of the quality of this simulation, Figures 5 and 6 display simulations of some of the other voltammograms of Figure 3. The only parameter that varied among these simulations was the photocurrent I_L. The values of A and I_o were fixed according to the simulation results of Figure 4b, and values for all other nonadjustable parameters

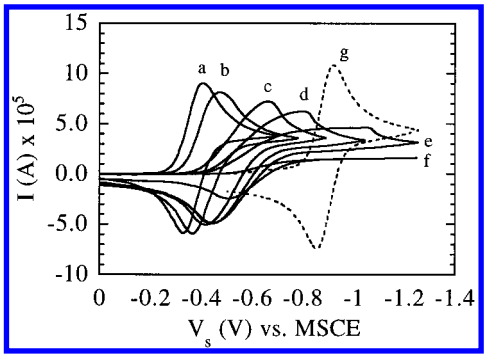

Figure 7. Cyclic voltammograms of a 1.5 Ω-cm *p*-Si photoelectrode ($A_s = 0.0583$ cm^2) in CH_3CN containing 4.5 mM $CoCp_2PF_6$ and 1.0 M $TEABF_4$ for various values of the light intensity I_L. The scan rate of the applied potential was 100 mV s^{-1}, and $E^{o\prime}$ was measured as −0.89 V versus MSCE. Cathodic currents are positive. Curve a: $I_L = 1.60 \times 10^{-3}$ A. Curve b: $I_L = 5.32 \times 10^{-4}$ A. Curve c: $I_L = 1.11 \times 10^{-4}$ A. Curve d: $I_L = 6.58 \times 10^{-5}$ A. Curve e: $I_L = 4.48 \times 10^{-5}$ A. Curve f: $I_L = 1.72 \times 10^{-5}$ A. The cyclic voltammogram of a Pt electrode ($A_s = 0.0633$ cm^2) immersed in the same electrochemical cell is also shown (curve g).

were as listed in Table 1. In general, the fits were outstanding, especially given the rather complicated wave shapes that were observed at low light intensities.

D. Cyclic Voltammetry of Semiconductor Electrodes. Two semiconductor electrode systems were investigated to obtain data suitable for a quantitative simulation of the voltammetry. These systems consisted of the *n*-Si/1 mM Me_2Fc−1.0 M $LiClO_4$−CH_3OH contact and the *p*-Si/1.2 mM Me_2-$CoCp_2PF_6$−1.0 M $TEABF_4$−CH_3CN contact. These junctions are known to obey the ideal semiconductor model in contact with the solvent/redox couple combinations employed herein (albeit at higher ratios of the concentration of the redox couple relative to the photogenerated carrier flux),[10,12,18−22] and such systems have been shown to be remarkably stable, efficient, and well behaved in their steady-state current−voltage properties. Furthermore, the effects of solution redox species concentrations on the interfacial transport rates for the *n*-Si/$Me_2Fc^{+/0}$−CH_3OH system have been found to be negligible for several different ratios of Me_2Fc/Me_2Fc^+.[10,18] This behavior suggests that the *I*−*V* data collected at high concentrations of redox reagents would be a useful indicator of the diode properties at the low redox concentrations required for cyclic voltammetry.

Cyclic voltammograms for the *n*-Si/1.0 mM Me_2Fc−1.0 M $LiClO_4$−CH_3OH contact deviated appreciably from those obtained at the Pt/1.0 mM Me_2Fc-1.0 M $LiClO_4$−CH_3OH interface, even at high light intensities. The ratio of anodic to cathodic peak current, I_{pa}/I_{pc}, equalled 1.3 for the *n*-Si/1.0 mM Me_2Fc−1.0 M $LiClO_4$−CH_3OH contact, whereas it was 1.0 for a Pt electrode immersed into this same solution. Furthermore, the peak-to-peak separation, ΔE_p, for the *n*-Si electrode was 114 mV at $v = 100$ mV s^{-1}, compared with the value of $\Delta E_p = 65$ mV obtained for the Pt metal electrode. Because of these discrepancies, which likely arise from an incomplete stabilization of the surface to oxidation under the conditions that are required for a cyclic voltammetric experiment (low redox concentration and high hole flux to the solid/liquid interface), no attempts were made to simulate this system using the reversible electrode/diode model.

The second semiconductor/liquid junction system investigated was the *p*-Si/cobaltocene$^{+/0}$ ($CoCp_2^{+/0}$)−CH_3CN contact, and this system proved more tractable. Figure 7 displays the cyclic voltammetric current−voltage behavior of a 1.5 Ω-cm resistivity *p*-Si photoelectrode ($A_s = 0.0583$ cm^2) in CH_3CN containing 4.5 mM $CoCp_2PF_6$ and 1.0 M $TEABF_4$. The cyclic voltammograms for the *p*-Si/CH_3CN−$CoCp_2^{+/0}$ system were qualitatively similar to the voltammograms expected theoretically. At high light intensities, the wave shape approached that of the conventional Pt metal electrode, with a difference between anodic and cathodic peak potentials, ΔE_p, of 75 mV and a cathodic peak width, $\Delta E_{p/2}$, of 65 mV. These values compared favorably with the $\Delta E_p = 66$ mV and $\Delta E_{p/2} = 60$ mV values obtained for a Pt electrode in the same solution.

Two approaches were employed to simulate the experimental cyclic voltammetric data. The first method involved the direct application of the nonlinear Levenberg−Marquardt least-squares method to the experimental data shown as curve f in Figure 7. For this particular voltammetric response, the dynamical impedance of the *p*-Si photoelectrode should dominate the current−voltage response of the electrochemical system, allowing the nonlinear fitting routine to extract values of the diode quality factor *A* and the reverse saturation current I_o. The parameters given in Table 2, determined in *Section IV.A* for a Pt electrode in this solution, were used as the standard unadjustable input parameters for the metal electrode component of the equivalent circuit model. The diode quality factor (*A*) and the reverse saturation current (I_o) were the only parameters allowed to vary. However, the Levenberg−Marquardt nonlinear least-squares algorithm was unable to converge to physically reasonable values of *A* and I_o for the data of Figure 7, curve f, so another approach was used to model the data.

In the second approach, the dynamic impedance of the semiconductor was independently determined for the solid/liquid contact of concern, and the resulting values for the diode quality factor and the reverse saturation current were used to generate simulated cyclic voltammograms. To determine the dynamic impedance, steady-state current−voltage curves were obtained for the *p*-Si/CH_3CN−0.20 M $CoCp_2PF_6$−1.0 mM $CoCp_2$−1.0 M $TEABF_4$ electrochemical cell at the values of I_L used in Figure 7. The diode quality factor *A* and the reverse saturation current I_o were then determined by fitting the corresponding steady-state current−voltage data to eq 11, after correcting for concentration overpotentials and solution series resistance losses.[7,9]

Figure 8 displays the simulated and experimental cyclic voltammetric response for these specific values of *A* and I_o and varying levels of illumination I_L. The quality of the fits between the simulated and the experimental data varied from good to only fair, with the best fits at high levels of illumination of the semiconductor. At high illumination, the match between simulated and experimental curves indicates that the system behaved as expected for a combination of diode and metal electrode circuit elements. At low illumination levels (high values of θ), the simulation failed to reproduce the peak positions, although the curve shapes were qualitatively correct. The source of these deviations at high θ is not fully understood at present, and the relatively poor quality of fit under these conditions indicates that further developments in the theory are required to describe the voltammetry of semiconductor/liquid contacts quantitatively.

V. Discussion

This equivalent circuit model provides useful insights into the voltammetry of hybrid semiconductor/electrode systems. It is not surprising that a simulated circuit consisting of a diode and a metal electrode is able to model with accuracy the very unusual waveshapes of a circuit consisting of the same electrical

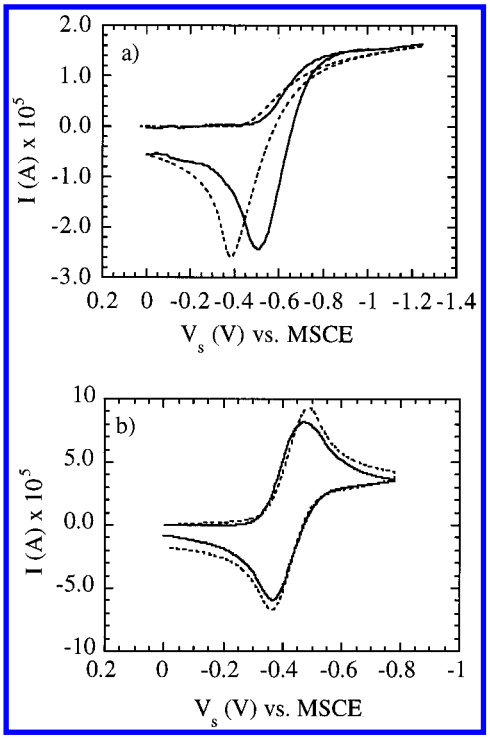

Figure 8. Experimental (solid curve) and simulated (dotted curve) cyclic voltammograms for the *p*-Si photoelectrode under conditions described in Figure 7. (a) $I_L = 1.72 \times 10^{-5}$ A; the specific values of $A = 4.61$, $I_o = 9.88 \times 10-7$ A used in the simulation were obtained from steady-state current−voltage data as described in the text. (b) $I_L = 5.32 \times 10^{-4}$ A; the specific values of $A = 4.90$, $I_o = 1.0 \times 10^{-5}$ A used in the simulation were obtained from steady-state current−voltage data as described in the text. Cathodic currents are positive. The values for all other parameters are given in Table 2.

elements. Moreover, the observation that this model can be used to predict the behavior of semiconductor electrodes is very encouraging. At high illumination levels, where the parameter θ is small, the simulated electrode response fit the experimental data well. At low illumination levels, the formalism did not fully describe the voltammetric waveshape, so discrepancies between simulated and actual voltammetry provide useful information to refine further the circuit model. In these regards, the simulation procedures developed earlier and modified herein to describe actual experimental cyclic voltammetric conditions were very successful.

Although it might appear that the model would have a sufficient number of adjustable parameters to obtain a close fit to any set of experimental cyclic voltammograms, this was not the case. The values of parameters were either measured independently or, in the case of A and I_o for the photodiode/Pt measurements, derived from fitting a cyclic voltammogram of the system of interest at a single illumination level. Figures 5 and 6 show that, for the diode/metal electrode system with all parameters fixed in this manner, reasonable agreement with the oddly shaped experimental voltammograms was attained over a 1000-fold range of the diode limiting current for a variety of illumination levels. The accuracy of these simulations was independently confirmed by the good match between the calculated and measured V_d versus V_s responses. This agreement between theory and experiment lends confidence to the modeling and simulation approach pursued herein to describe the voltammetry of these nonmetallic electrode systems.

The inability to simulate the experimental cyclic voltammetric data shown in Figure 7 for the *p*-Si/1.0 M $TEABF_4$−4.5 mM $CoCp_2PF_6$−CH_3CN electrochemical system at large θ is of significant interest. Although it would certainly have been possible to obtain satisfactory fits to the observed voltammetry by introducing a variable charge-transfer rate constant at each light intensity, this procedure would not have added physical insight into the behavior of the system and therefore was not pursued quantitatively. An assumption inherent in modeling a semiconducting electrode as a metal electrode/diode series combination is that the concentration ratio of oxidized/reduced species at the electrode surface is either controlled by the Nernst equation and offset by a relatively fixed photovoltage (i.e., the condition at low θ values) or is controlled by a combination of galvanostatic control and redox species mass transport (i.e., the conditions at high θ in the diode/electrode circuit and in the simulation). In actuality, it is likely that the effective capture velocity for a photogenerated charge carrier in the semiconductor being transferred to a redox species in the solution is dependent on the light intensity incident onto the semiconductor. Under conditions where a limited flux of minority carriers is being created by the illumination source, this intensity-dependent charge-transfer rate is predicted by a second-order rate law for the capture of photogenerated minority carriers by redox acceptors in the solution phase[23] (and is also in accord with, but does not by itself prove the validity of, the quasi-Fermi concept at semiconductor electrodes[24]). This situation of having an effective minority carrier capture velocity that depends on the light intensity, and of having to consider the kinetics of minority and majority carriers separately as opposed to parameterizing them into one effective rate constant for charge transfer between the solid and the redox species, is unique to the semiconductor electrode and is not present in the model diode/electrode circuit or in the simulations performed to date. We note that, to the extent that this shortcoming in the diode/electrode circuit is general to the modeling of actual semiconductor electrodes, the simulations presented previously at low light intensities (i.e., high θ values) for rotating disk electrodes and for the cyclic voltammetric behavior of surface-attached species at semiconductor electrodes[1,2] would also suffer similar limitations and thus would be useful in this regime only for providing a qualitative description of the electrochemical behavior of semiconductor electrodes. A more complete model, requiring a coupled description of generation, recombination, and transport in the semiconductor, as well as interfacial kinetic processes and diffusion of redox species in the electrolyte, would therefore apparently be required to describe completely the experimental voltammetry of semiconductor electrodes. We are not aware, however, of the availability of such a sophisiticated model at the present time in the literature, and further insight into the experimental cyclic voltammograms evidently will require such sophisticated treatments to describe even the simplest experimental systems reported to date.

In summary, the cyclic voltammetry of a model diode/electrode circuit has been shown to resemble that of an actual semiconducting photoelectrode in contact with an outer-sphere redox couple. The voltammetric response of the model diode/electrode circuit can be described quantitatively using a digital simulation of the response of each separate element. Such simulations have allowed an understanding of the voltammetric waveshapes for this system under arbitrary experimental conditions. At high light intensities, the voltammetry of semiconducting photoelectrodes is also well described by this equivalent circuit formalism. However, under low light intensities, further theoretical developments, including a complete treatment of the heterogeneous kinetics as a function of the charge carrier

concentration at the electrode surface, are required to satisfactorily describe the voltammetric waveshapes of such contacts.

Acknowledgment. We acknowledge the Petroleum Research Foundation and the Department of Energy, Office of Basic Energy Sciences, DE-FG-03-88ER13932LN, for support of this work. M. Lieberman also acknowledges the National Science Foundation, Grant CHE-9403134, for a postdoctoral fellowship. We are also grateful to Dr. S. Feldberg of Brookhaven National Laboratory for numerous discussions regarding simulation procedures and methodology for these systems.

References and Notes

(1) Santangelo, P. G.; Miskelly, G. M.; Lewis, N. S. *J. Phys. Chem.* **1988**, *92*, 6359.

(2) Santangelo, P. G.; Miskelly, G. M.; Lewis, N. S. *J. Phys. Chem.* **1989**, *93*, 6128.

(3) Gerischer, H. *J. Electroanal. Chem.* **1975**, *58*, 263.

(4) Bruckenstein, S.; Miller, B. *J. Electrochem. Soc.* **1982**, *129*, 2029.

(5) Decker, F.; Fracastoro-Decker, M.; Badawy, W.; Doblhofer, K.; Gerischer, H. *J. Electrochem. Soc.* **1983**, *130*, 2173.

(6) Bruckenstein, S.; Rosamilia, J. M.; Miller, B. *J. Phys. Chem.* **1985**, *89*, 677.

(7) Bard, A. J.; Faulkner, L. R. *Electrochemical Methods: Fundamentals and Applications*; John Wiley & Sons: New York, 1980.

(8) Feldberg, S. In *Electrochemistry Calculations, Simulations, and Instrumentation*; J. Mattson, Ed.; Marcel Dekker: New York, 1972.

(9) Casagrande, L. G. Ph.D. Thesis, Stanford University, 1988.

(10) Rosenbluth, M. L.; Lewis, N. S. *J. Am. Chem. Soc.* **1986**, *108*, 4689.

(11) Sawyer, D. T.; Roberts, J. L. *Experimental Electrochemistry for Chemists*; Wiley: New York, 1974.

(12) Rosenbluth, M. L.; Lieber, C. M.; Lewis, N. S. *Appl. Phys. Lett.* **1984**, *45*, 423.

(13) Marquardt, D. W. *J. Soc. Indust. Appl. Math.* **1963**, *11*, 431.

(14) Bevington, P. R. *Data Reduction and Error Analysis for the Physical Sciences*; McGraw-Hill: New York, 1969.

(15) Press: W. H.; Flannery, B. P.; Teukolsky, S. A.; Vetterling, W. T. *Numerical Recipes: The Art of Scientific Computing*; Cambridge University: Cambridge, 1986.

(16) Adams, R. N. *Electrochemistry at Solid Electrodes*; Marcel Dekker: New York, 1967.

(17) Santangelo, P. G. Ph.D. Thesis, Stanford University, 1991.

(18) Rosenbluth, M. L. Ph.D. Thesis, Stanford University, 1988.

(19) Rosenbluth, M. L.; Lewis, N. S. *J. Phys. Chem.* **1989**, *93*, 3735.

(20) Lewis, N. S. *J. Electrochem. Soc.* **1984**, *131*, 2496.

(21) Lieber, C. M.; Gronet, C. M.; Lewis, N. S. *Nature* **1984**, *307*, 533.

(22) Abrahams, I. L.; Casagrande, L. G.; Rosenblum, M. D.; Rosenbluth, M. L.; Santangelo, P. G.; Tufts, B. J.; Lewis, N. S. *New J. Chem.* **1987**, *11*, 157.

(23) Lewis, N. S. *Annu. Rev. Phys. Chem.* **1991**, *42*, 543.

(24) (a) Gerischer, H. In *Solar Energy Conversion. Solid-State Physics Aspects*; Seraphin, B. O., Ed.; Springer-Verlag: Berlin, 1979; Vol. 31, p 115. b) Reineke, R.; Memming, R. *J. Phys. Chem.* **1992**, *96*, 1317. (c) Tan, M. X.; Kenyon, C. N.; Kruger, O.; Lewis, N. S. *J. Phys. Chem.* **1997**, *101*, 15, 2830.